WCAP-18904-NP
Revision 0

November 2023

Critical Power Experiments and D6 CPR Correlation for TRITON11® Fuel

Westinghouse

WCAP-18904-NP
Revision 0

Critical Power Experiments and D6 CPR Correlation for TRITON11® Fuel

Uffe Bergmann *
Fuel Product Engineering

Jean-Marie Le Corre *
Next Generation Methods

November 2023

Reviewer: Carl Adamsson *
Next Generation Methods

Kjell Bergman *
BWR Safety Analysis

Nathaniel J. Mackereth *
Licensing Engineering

Approved: Magnus Limbäck *, Manager
Fuel Materials Innovation

Zachary S. Harper, Manager *
Licensing Engineering

*Electronically approved records are authenticated in the electronic document management system.

Westinghouse Electric Company LLC
1000 Westinghouse Drive
Cranberry Township, PA 16066, USA

ABSTRACT

This report describes the development and validation of a new critical power ratio (CPR) correlation for Westinghouse **TRITON11**® boiling water reactor (BWR) fuel assemblies. This new CPR correlation is referred to as D6. The D6 CPR correlation and the bases for its acceptance are presented in this report.

TABLE OF CONTENTS

LIST OF TABLES

LIST OF FIGURES

ABBREVIATIONS

AM	Additive Manufacturing
AOO	Anticipated Operational Occurrence
BHL	Beginning of Heated Length
BWR	Boiling Water Reactor
CPR	Critical Power Ratio
E	East
EHL	End of Heated Length
LUA	Lead Use Assembly
N	North
OLMCPR	Operating Limit Minimum CPR
PCI	Pellet Cladding Interaction
PLR	Part-Length Rod
S	South
SLMCPR	Safety Limit Minimum CPR
TC	Thermocouple
W	West

1 INTRODUCTION AND EXECUTIVE SUMMARY

This report describes the development and qualification of a new CPR correlation for **TRITON11®** fuel, Westinghouse's next generation 11×11 BWR fuel product. The new CPR correlation is named "D6". The D6 CPR correlation was established based on a complete scope of dryout testing in the Westinghouse FRIGG loop with **[** **]**[a,c]. It is applicable to **TRITON11** reload fuel and lead use assemblies (LUAs) delivered to BWRs in United States of America.

1.1 TRITON11 FUEL DESIGN

The **TRITON11** fuel is the latest fuel design following an evolutionary line of SVEA-96 type designs, i.e., the SVEA-96, SVEA-96+, SVEA-96 Optima, SVEA-96 Optima2, and **SVEA-96 Optima3™** designs. Those fuel designs are all composed of four sub-bundles with a 5×5 lattice configuration with one fuel rod missing, separated by the characteristic SVEA water cross. With the introduction of **TRITON11** fuel, the SVEA channel concept is abandoned, making room for another row of fuel rods when transitioning to an 11×11 lattice design. The layout of the **TRITON11** fuel assembly is shown in Figure 1-1. The assembly includes three circular water rods, centrally located and passing non-boiling water, as well as 109 fuel rods of which 91 are of full length, 8 of 2/3 length, and 10 of 1/3 length. The **TRITON11** fuel bundle is supported laterally by 10 spacer grids with optimized mixing vane features.

The key incentives for developing the **TRITON11** design were to support the current industry move towards higher energy cycles and higher burnup, as well as the requests for increased operational flexibility (allowing extended load follow) and improved fuel reliability. Careful considerations were given to the overall reliability of the new design to further reduce the risk of fuel failures.

Important reliability features introduced and proven by the **SVEA-96 Optima3** design have been maintained in the **TRITON11** design:

- Enhanced debris failure resistance and structural strength of spacer grids based on a unique sleeve-type cell technology.
- Elimination of potential cladding bending stresses by having all fuel rods resting freely on top of the bottom tie plate and extending through a top spacer (replacing the top tie plate).
- Excellent dimensional stability and low hydrogen pickup of **Low Tin ZIRLO™** material used for fuel channel and water rods.
- Successful ZrSn-liner inner component of fuel cladding.
- High-density **ADOPT™** pellet.
- Enhanced efficiency of the new **StrongHold®** additively manufactured (AM) debris filter.

The **TRITON11** fuel incorporates a robust mechanical design concept based on lifting via the three water rods, hence leaving all fuel rods free of any external handling loads. Further improvements in fuel reliability are enabled by:

- 10% reduction in average fuel rod linear heat generation rate, improving margins to most fuel rod design criteria and pellet cladding interaction (PCI).

- Spacer frame design with improved debris resistance.
- Redundant bundle lift and spacer capture functions provided by the three (non-U bearing) water rods.

1.2 TEST CONDITIONS IN FRIGG LOOP

When performing dryout testing of the **TRITON11** design in the FRIGG loop, all fuel assembly components within the heated section of the fuel are included and very closely resemble those used in **TRITON11** fuel assemblies operated in BWRs. In particular, all 109 fuel rods are simulated by use of electrically heated rods. The use of indirectly heated rods (with the electrical current passing through an internal filament, rather than through the outer cladding), connected to several individual rectifier units, makes it possible to control the relative (lateral) rod power distribution in a simple manner to test a wide range of lateral power distributions, without having to dismantle and rebuild the test bundle. In addition, a high-precision stainless steel flow channel was manufactured for the **TRITON11** testing, having very precisely adapted and known inner dimensions.

The objectives of the dryout tests and the CPR evaluation program were as follows:

- Experimentally determine the steady-state and transient critical power performances of the **TRITON11** assembly over a wide range of simulated BWR operating conditions. The range of BWR operating conditions must be sufficient to predict the critical power behavior of the **TRITON11** fuel assembly over the entire steady-state and transient operating ranges of BWRs for design and licensing applications.
- Develop the D6 CPR correlation for **TRITON11** fuel to adequately predict the steady-state critical power database. Establish appropriate biases and uncertainties for licensing applications. The correlation shall provide best-estimate CPR values for steady-state applications.
- Ensure that the D6 CPR correlation for **TRITON11** fuel provides adequate prediction of critical power during transients. This confirmation is performed by comparing the CPR predictions for transient conditions with the available transient critical power test data. The Westinghouse methodology for performing this confirmation is demonstrated with the BISON code [1].

The test matrix was selected to cover the typical steady-state and transient operating conditions expected for BWRs of ASEA, KWU, GE BWR/2-6 and ABWR types, including off-nominal conditions to allow application to accident conditions. Particular emphasis has been put on capturing the dependence on lateral power distributions within the bundle since this is expected to be the major bundle-specific effect.

[

]^{a,c}

The present D6 CPR correlation was developed based on [ ]^{a,c} steady-state critical power data points, [ ]^{a,c} points with [ ]^{a,c} and [ ]^{a,c} points with [ ]^{a,c}, and validated against [ ]^{a,c} transient measurements, [ ]^{a,c} with [ ]^{a,c} and [ ]^{a,c} with [ ]^{a,c}. The same [ ]^{a,c} steady-state data points that were used for optimizing the correlation coefficients were also used for investigating the resulting correlation performance trends. When determining the correlation mean and standard deviation errors, the database was randomly divided into one subset with [ ]^{a,c} of the data used for training and the remaining subset of [ ]^{a,c} of the data was reserved for validation. This process was repeated many times and the sample average mean and standard deviation errors of the validation data subsets were used to determine the final correlation performance statistics.

In addition to the data points dedicated for development and validation, a flow series of repeated data points, i.e., with the same loop operation parameters and the same (or very similar) lateral power distribution, was taken during each individual rectifier connection. This data served to verify that loop conditions were stable, and the results were reproducible.

The **TRITON11** dryout tests include measurements of critical power at pressure between [ ]^{a,c}, inlet sub-cooling between [ ]^{a,c} and mass flux between [ ]^{a,c}. The critical power measurements were performed for approximately [ ]^{a,c} different lateral power distributions to capture the influence on critical power of various local peaking factors and various peak power rod locations.

The data for **TRITON11** show similar trends as function of mass flux, inlet sub-cooling, pressure, axial power profile, and local power peaking (R-factor) as previous Westinghouse BWR fuel designs.

1.3 D6 CPR CORRELATION MODEL AND VALIDATION

The D6 CPR correlation model for **TRITON11** fuel inherits the same basic correlation form as the D5 CPR correlation used for **SVEA-96 Optima3** fuel [2]. The expression for critical quality as function of mass flux, pressure, sub-cooling, axial power profile transformation (I_2), and R-factor is identical. [1] The differences between the D5 and D6 CPR correlations, apart from assigning new values to the regression coefficients by fitting against the FRIGG data, are solely in the R-factor model. In addition to the obvious expansion from 5×5 to 11×11 rod lattice geometry, the D6 R-factor model includes a new R-factor term that accounts for **[**

]^{a,c}

The D5 correlation concept introduced new mechanistically-motivated features and has a form that departs from earlier CPR correlations, [3] and [4]. The improved features inherited by the D6 CPR correlation can be summarized as follows:

- Proper qualitative behavior is assured by the correlation form itself, rather than the values of its regression coefficients. This improves the correlation performance when extrapolating to conditions outside the test database.

- CPR correlation complexity is dramatically reduced (less regression coefficients) by use of exponential functions (rather than polynomials) with appropriate asymptotic behaviors derived from measured trends in critical power. This ensures a robust correlation behavior under all conditions, in particular during transients.

- Effects of axial power distribution are accounted for through a transformation of the axial power profile – the so-called I_2 integral – which can be derived from physical considerations of the mass balance in the liquid film and is a refinement of previous concepts based on annular length and boiling length.

- Generalization of the R-factor formulation to better capture the influence of part-length rods (PLRs) and to enable utilization of the complete 3-dimensional pin power distribution for a **TRITON11** fuel bundle as calculated by pin power reconstruction techniques in a licensed core simulator (e.g. POLCA7, [5]). The use of pin power reconstruction for CPR allows to more accurately capture the effects of local power conditions in the core by including the perturbations in the neutron flux caused by neighboring bundles, control blades inserted in neighboring cells and leakage effects near the core periphery.

Based on these new features, the D5 and D6 CPR correlations offer significant improvements to nuclear safety by allowing more accurate determination of the margins to dryout for every fuel rod in the core.

The ability of the correlation to match the experimental data is reflected by the statistics of the relative deviation between the predicted and measured critical power over the subsets of **[ ]^{a,c}** of the database used for validation. The present D6 CPR correlation for **TRITON11** fuel predicts the measured steady-

[1] **[**

]^{a,c}

state critical powers with a mean error of [ ]^{a,c} and a standard deviation error of [ ]^{a,c} over the steady-state database used for validation.

[

]^{a,c} Transient tests with power increase and/or flow reduction were included. The evaluation in Section 6 provides a demonstration, using the BISON dynamic system transient code, that the D6 CPR correlation, developed based on steady-state data, accurately predicts CPR behavior under transient conditions. The same methodology can also be used to confirm that CPR changes during transient events are accurately treated in other licensed transient codes.

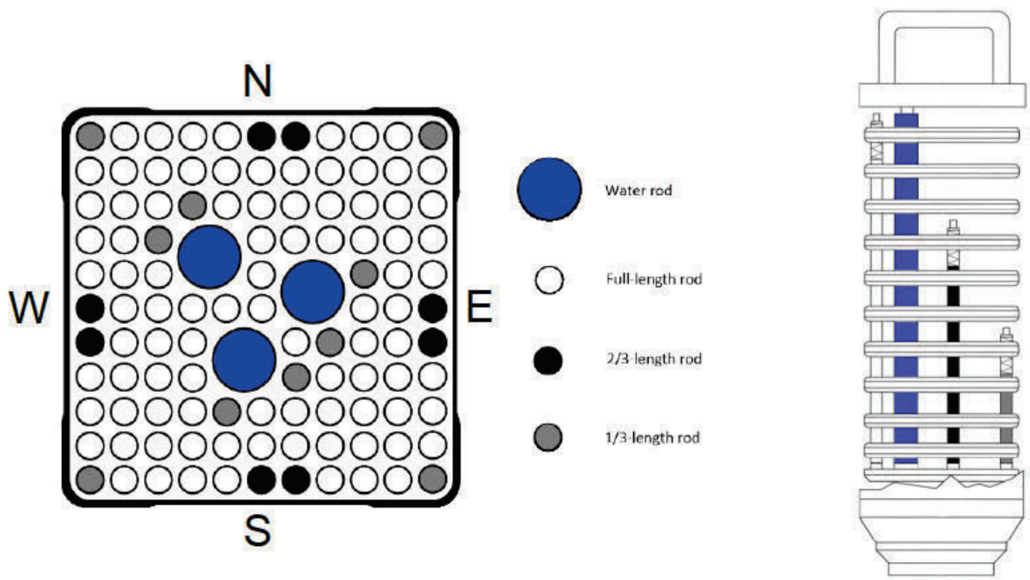

Left panel: **TRITON11** fuel lattice cross-section geometry. In the reactor, the **TRITON11** fuel bundle is always oriented with the control rod in the NW corner.
Right panel: **TRITON11** fuel bundle geometry.

Figure 1-1. TRITON11 Fuel Bundle Diagram

2 TEST FACILITY

2.1 GENERAL DESCRIPTION

The **TRITON11** critical power tests were performed in the FRIGG loop at the Westinghouse fuel thermal-hydraulic laboratory in Västerås, Sweden. The final fuel qualification tests were performed during 2020 with test rods of **[**

]a,c The FRIGG loop has been utilized for many years to perform thermal-hydraulic tests in support of the Westinghouse BWR nuclear fuel program. An overview of the FRIGG test facility and **TRITON11** thermal-hydraulic testing program is documented in [6].

A diagram of the FRIGG loop is shown in Figure 2-1. The loop includes a main circulation loop with the test section, a cooling circuit and a purification system. The head of the main circulation pump can be continuously controlled by means of a variable speed motor. When steam is produced in the test section, the loop pressure is controlled by regulating the cold water flow to spray nozzles in the condenser. Heat is removed by a heat exchanger in the cooling circuit from which water is pumped to the spray nozzles. During start-up and heat balance tests, the loop is filled with water and the pressure is regulated by balancing the amount of water by means of the feed-water pump and a drainage valve. The inlet sub-cooling is controlled by feeding water from the cooling circuit into the main circulation loop upstream of the pump.

The loop is designed for a maximum pressure of 100 bar and a maximum temperature of 311°C. Carbon steel is used throughout as construction material. Demineralized and degassed water is used for filling the loop and water quality is carefully controlled. Purification is performed continuously during the tests to keep water quality within specified limits. Normally, water conductivity is in the range of 0.15 – 0.30 µS/cm.

2.2 TEST SECTION

The test section consists of a pressure vessel, a high-precision stainless steel flow channel and a full **TRITON11** bundle with 109 heater rods placed according to the lattice design in Figure 1-1. By use of a stainless-steel flow channel, the channel inner dimensions during loop operation can be controlled more accurately as compared to a zircalloy flow channel. Pressure taps are connected through the flow channel at different elevations and the pressure transmission lines are brought out of the test section through an instrumentation ring.

An orifice plate is installed at the inlet to the flow channel to provide more even distribution of flow into the channel. The orifice plate has a loss coefficient of five velocity heads.

The heater rods are laterally supported by eight Inconel spacer grids of **TRITON11** design within the heated length. They are denoted SP1 through SP8 and are numbered from the top down (i.e., SP1 being the uppermost). Photos of the three different types of **TRITON11** spacers used for SP1 through SP8 are shown in Figure 2-2. Additional support spacers (not affecting the critical power performances) are positioned at the inlet and outlet of the test section. The axial locations of the spacer grids are shown in Figure 2-3. Both spacer designs and spacer elevations are consistent with **TRITON11** reactor fuel bundle.

[

]^{a,c} The spacers fulfil all relevant requirements from manufacturing tolerances.

[

]^{a,c}

The pressure vessel top flange contains pressure seals similar in design to valve stem packing seals which retain the heater rods in fixed positions. The difference in thermal expansion between the heater rods and the pressure vessel is offset via O-ring pressure seals in the bottom flange.

The actual (measured) dimensions of the FRIGG test bundle are compared with nominal dimensions for a **TRITON11** reactor fuel bundle in Table 2-1. The relevant dimensions that may influence dryout all closely resemble those of **TRITON11** reactor fuel. When accounting for the slightly different thermal expansion properties of the stainless steel vs zircalloy flow channels and FRIGG heater rods vs real fuel rods, the corresponding cold flow area in the lower part of the FRIGG test section is [ ]^{a,c}, as compared to [ ]^{a,c} for the reactor fuel bundle. Differences in flow area are specifically accounted for through the mass flux which is an input variable to the CPR correlation.

As indicated in Table 2-1, **TRITON11** fuel may be supplied to reactors with slightly different heated lengths. In all cases, the distances from BHL to each spacer within the heated length are the same. Consequently, the distance from the EHL to the uppermost active spacer varies somewhat depending on reactor. Since the D6 CPR correlation does not include an explicit model of the spacers, the spacer positions in the test bundle were chosen conservatively to represent the most limiting case in terms of critical power, corresponding to the longest distance from the uppermost active spacer to EHL. This case is applicable to GE BWR 4-6 type plants. This means that for the slightly shorter fuel used in GE BWR 2-3, ASEA and KWU type plants the distance from the uppermost active spacer to EHL is shorter compared to the test bundle. The critical power being most sensitive to integrated heat flux, rather than local heat flux, a shorter distance to the spacer below can only result in a (slightly) higher critical power due to the higher enhancement of water drop deposition. Hence, the experimental setup is conservative for the case of shorter fuel.

In addition to the spacer distance effects discussed above, there are the differences in power distribution due to the differences in heated length. This small effect is fully captured by the I_2 concept of the D6 CPR correlation. The heater rods were fabricated with slightly varying lengths, but all rods of the same type were mounted in the test assembly to define a common EHL relative to the reference BHL.

The mechanical lengths of the PLRs are the same in all reactor fuel bundles since they are coupled to the positions of the spacer levels. The same physical lengths were used in the test bundles. The heated lengths of the PLRs, on the other hand, may differ slightly between reactor fuel bundles due to possible differences in the plenum lengths. This means that there can be minor differences in EHL for PLRs between the test bundle and reactor fuel. The EHL is accounted for explicitly in the performance of PLRs according to the D6 R-factor model. Since dryout typically occurs well above the PLRs, the effect is judged to be insignificant for the full-length rods.

In addition, **[**

] a,c

2.3 HEATER RODS

Figure 2-4 shows the heater rod numbering scheme that identifies the rod locations in the FRIGG test bundle. Figure 2-5, Figure 2-6, Table 2-2, and Table 2-3 show the heater rod axial power shapes used in the two test campaigns. **[**

] a,c

The heater rods used in the tests are indirectly heated. Each heater rod contains a heater element, electrical insulation, Monel K-500 cladding, and three to eight thermocouples (TCs) used as dryout detectors. The heater element is made from a Monel K-500 tube. The heater element terminals consist of a solid nickel transition piece welded to the Monel tube at one end, and to a copper electrode brazed to the Monel tube at the other end. The heater-rod non-uniform axial power profiles were generated by laser cutting a spiral on the Monel tube with a variable pitch.

The power ratings of the heater rods in the test sections at 380V DC are as follows:

[ ] **a,c**

Design sketches of a full-length heater rod and a part-length heater rod are shown in Figure 2-7 and Figure 2-8, respectively.

[

] a,c

[

]a,c

The electrical insulation was machined from solid boron nitrite (BN) pieces. After the BN sleeves were assembled over the heater element, grooves were cut axially to hold the TCs in position. Then the heater element assembly was inserted into the oversized cladding tube. The final heater rod dimensions were obtained by swaging the heater assembly to its final dimensions. The swaging operation also provided good contact between the heater element, the insulation material, and the cladding inner surface assuring good heat transfer with low variability from the heating element to the cladding surface.

The TCs are embedded between the cladding and the insulation sleeves. The full-length rod TC extensions are routed from the top end of the heater rod, and the part-length extensions are routed from the bottom end. The TCs used were 0.51 mm unground, Inconel 600-sheathed, type K, with magnesium oxide (MgO) insulation. The TC wire used was of premium grade. The TC tips were backfilled with BN powder and compacted by swaging to provide a faster response to temperature changes.

[

]a,c

2.4 POWER SUPPLY AND CONTROL

Electrical power to the heater rods was supplied by a 15 MW DC electrical power system operating at 0-400 V. The system consisted of seven units (rectifiers), rated at 1.8 kA each, two rectifiers rated at 10 kA each and two rectifiers rated at 12 kA each.

The upgraded FRIGG loop has a very flexible system for connecting the individual heater rods to selected units. This configuration provides the capability to conveniently obtain numerous combinations of relative rod powers by adjusting the computer signals that control the voltage across each unit. It is this capability that allows a thorough determination of R-factors, providing the relative dryout sensitivity of each fuel rod as well as sensitivity to lateral power peaking.

2.5 INSTRUMENTATION

The variables defining the operating conditions during the tests consist of pressure, inlet sub-cooling, power, and mass flow rate. These variables and the methods by which they are measured are discussed below. The measurement accuracy for each variable is given as $\pm 1\sigma$ for a normal distribution.

[

]a,c

The above accuracies in the major variables yield a contribution from measurement uncertainty to CPR of [ ]a,c obtained by standard error propagation based on the above estimated accuracies in the major variables, multiplied by corresponding generic CPR sensitivity coefficients. This has the following meaning. If the CPR correlation model were “exact” (zero model uncertainty), the uncertainties in the measured input variables to the correlation and the uncertainty in the measured critical power would together give rise to relative differences in the predicted and measured critical powers with a standard deviation of [ ]a,c

2.6 DATA ACQUISITION SYSTEM

The data acquisition system is sketched in Figure 2-11. Signals reflecting important parameters (e.g., temperature, voltage, current, differential pressure, and mass flow) are connected to NI PXIe data loggers collecting data at 25 Hz. For steady-state tests, the measurements are averaged to 5 Hz, further averaged every 5 time steps at the dryout conditions. For transient tests, the sampling frequency of 25 Hz is directly used.

In addition to the data collecting function, the computer was also used as a dryout monitor by utilizing software that allows it to recognize a temperature rise over a given time in up to 832 heater rod TCs. In this way, the computer identified all TCs indicating dryout. **[**

]^{a,c} The detection method of dryout during transients is discussed in Section 6.3.4.

In addition to the dryout criterion, three different alarm limits were used to protect the heater rods during steady-state measurements. A rate of temperature increase greater than 50°C/s, or an absolute temperature above 550°C, automatically triggered the rectifiers to reduce bundle power by 25%. A rate of temperature increase greater than 75°C/s caused the bundle power to be shut off completely. The temperature monitoring function must be in operation before power is provided to the test section.

For testing in transient mode with predefined excursions in power and/or flow over a limited period of time (< 10 s), the alarm limits were adapted to allow a faster temperature rise because it would be automatically quenched by a predefined power reduction at the end of the transient.

2.7 CRITICAL POWER TESTING PROCEDURE

The measuring instruments and the data acquisition system used are discussed in the previous Sections 2.5 and 2.6. The tests were recorded in blocks with a maximum size of 2400 samples of each parameter, which corresponds to 2400 seconds at a sampling frequency of 1 Hz. Each block generally included several critical power measurements at different mass flows.

The procedure for obtaining a steady-state critical power data point was as follows:

1. The test identification number was entered into the computer.

2. The targeted relative rod power distribution was entered into the computer, which established the corresponding rectifier settings. Deviations between the target and actual relative rod powers were monitored in real time and were verified to be within acceptable limits.

3. The targeted bundle inlet sub-cooling temperature, system pressure, and mass flux were established.

4. [

]a,c All TCs were connected to the data loggers, and their outputs were recorded during the test. In addition, selected TC outputs of interest were displayed on a monitor in the control room.

2.8 COMPARISON TO OUTSIDE SOURCE

As part of a Technical Development Agreement between ASEA-ATOM (AA) and General Electric (GE), a series of comparative full-scale dryout experiments were performed at the AA FRIGG and GE ATLAS loop facilities during the late 1970's. Comparisons between FRIGG and ATLAS data, and between correlations based on the corresponding data, were made. The data included measurements of critical power and pressure drop. The measurement procedures were those specific to each test facility.

One important objective was to duplicate the same test conditions (bundle geometry, heat flux distribution and spacer design) as far as realistically possible, make a direct comparison of the measured critical power levels and look for evidence of any laboratory bias or trends. This was the particular objective of the Program Statement AAGE-104 where a 16-rod bundle tested by GE in the ATLAS loop was duplicated and tested by AA in the FRIGG loop. The selected bundle was a 4×4 subset of the 7×7 lattice type with corner peaking and cosine axial heat flux distribution. The same spacers were applied in the two tests. The experimental procedures were, as far as possible, the same as applied in large bundle tests. Direct comparison of the measured critical power levels showed very consistent trends. [

]a,c A discrepancy of that order could well be explained by the combined measurement errors in the two series of experiments and, hence, it was concluded that there was no evidence of any laboratory bias.

Table 2-1. Dimensions at Room Temperature for FRIGG Test Bundle vs Reactor Fuel Bundle

Parameter	FRIGG test bundle (as measured)	Reactor fuel bundle (nominal)

a,c

Table 2-2. Normalized Rod Axial Power Distributions over the Heated Lengths (Discretized in 25 Uniform Nodes over a Reference Length of 3.81 m) for [ ]a,c

[ ]a,b,c

Table 2-3. Normalized Rod Axial Power Distributions (Discretized in 25 Uniform Nodes over a Reference FLR Length of 3.81 m) for [ ][a,c]

[ ] a,b,c

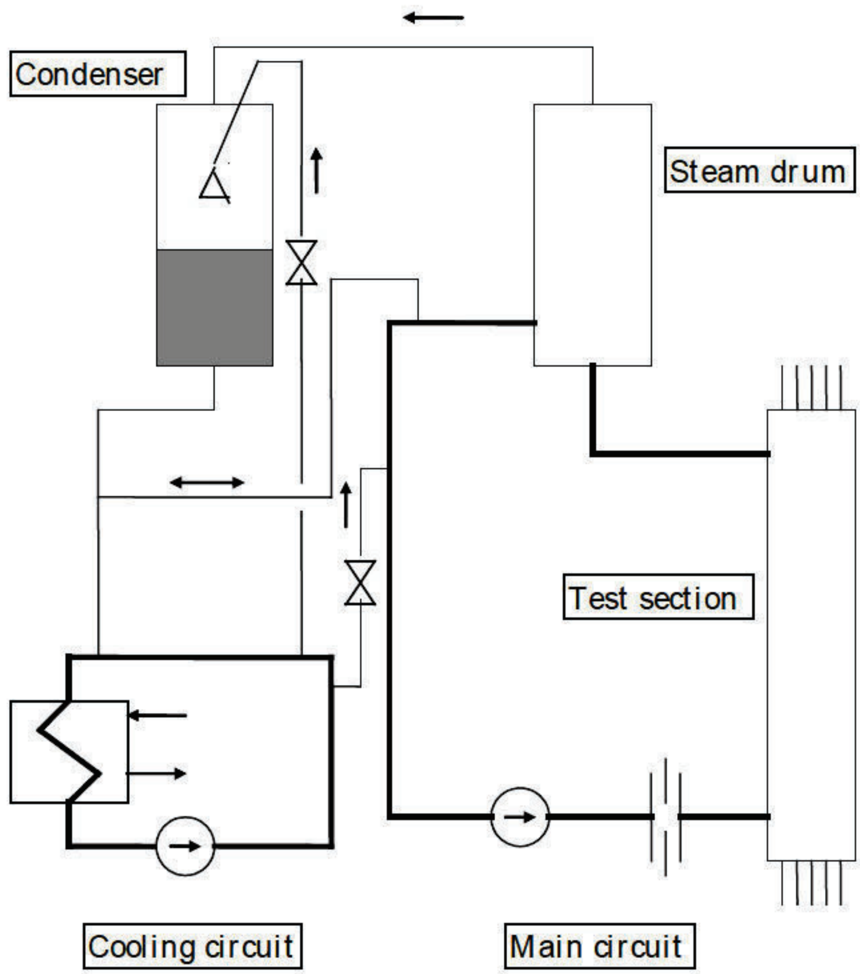

Figure 2-1. FRIGG Loop Diagram

[ ]a,c

Figure 2-2. TRITON11 Spacer Grid

a,c

Figure 2-3. Axial Positions of Spacer Grids

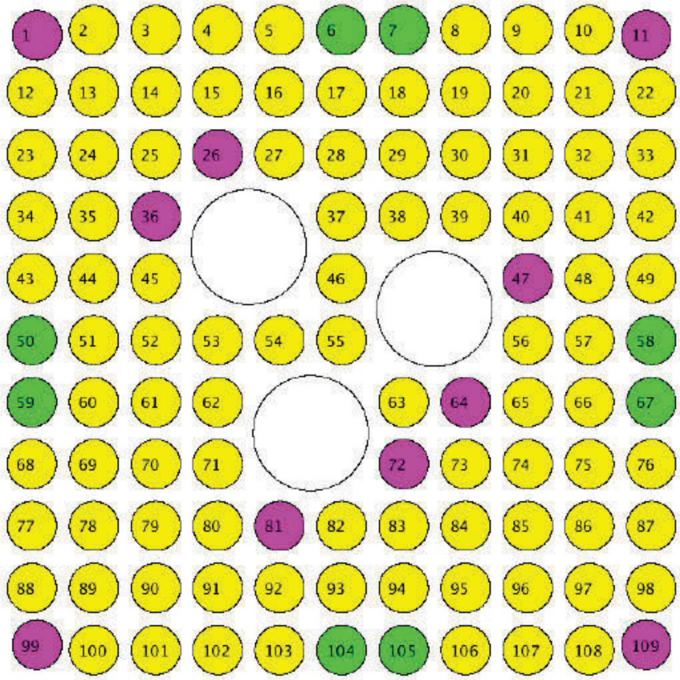

Figure 2-4. Numbering of Rods in the TRITON11 Bundle

[ ]a,b,c

Figure 2-5. Rod Axial Power Shapes with [ ]a,c (FRIGG Test Campaign)

a,b,c

Figure 2-6. Rod Axial Power Shapes with [ ][a,c] (FRIGG Test Campaign)

a,c

Figure 2-7. Full Length Heater Rod Design

a,c

Figure 2-8. Part-Length Heater Rod Design

a,c

Figure 2-9. Azimuthal Positioning of Thermocouples at all Elevations for the [ ]a,c Test Campaign

a,c

Figure 2-10. Azimuthal Positioning of Thermocouples at all Elevations for the [ ]^{a,c} Test Campaign

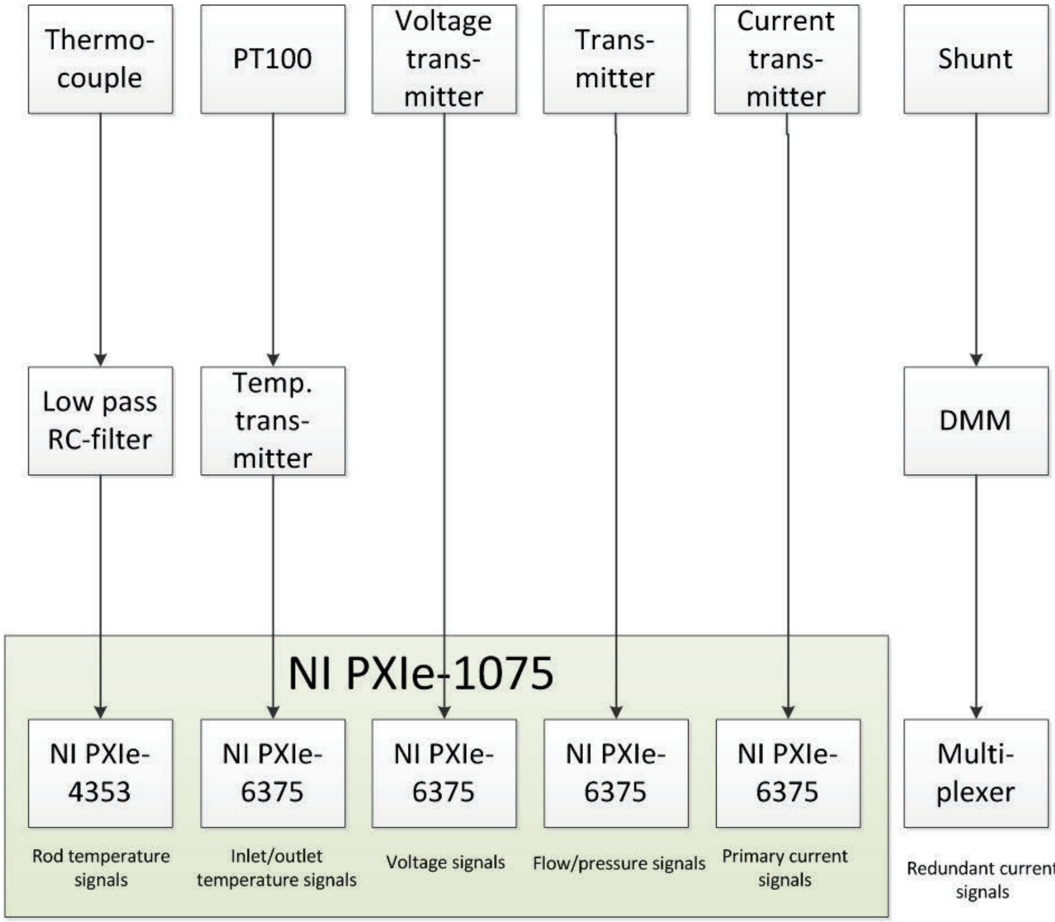

Figure 2-11. Data Acquisition System

3 TEST PROGRAM

As discussed in Section 2, the test program included two separate test campaigns. The campaigns were performed with full-size 109-rods **TRITON11** bundle test sections. The two test campaigns mainly differ by the axial power shapes provided by the heater rods. [ ]a,c

The database for each axial power profile consists of several categories (see below). In all categories (except Type 1), and for each considered radial power distribution, a series of flow levels were included. [ ]a,c

The number of steady-state data points and different lateral power distributions obtained in each of the two test campaigns are summarized in Table 3-1. Each data point is associated with one of five types of rectifier connection/lateral power distribution which indicates the purpose of the given measurement. The categories are:

[ ]a,c

For each condition of lateral power distribution, pressure and inlet sub-cooling tested under the categories 1-5, several [ ]a,c data points were taken to cover a wide range in mass flow. The number of data points within each category is given in Table 3-2.

Of the collected data points, **[ ]**^{a,c} points were not used for development or for evaluating the correlation bias and standard deviation since they were performed at almost identical conditions as other data points that were included. It is of no interest to dilute the development database and correlation statistics with additional data points containing the same information. Of the **[ ]**^{a,c} excluded data points, **[ ]**^{a,c} were taken deliberately as repeat points with a uniform lateral power distribution to verify that test loop conditions did not change significantly over time and the results were reproducible. This allows a direct verification of the experimental uncertainty on critical power (see Sections 2.5 and 3.3). The remaining **[ ]**^{a,c} excluded data points were taken as initial conditions for transient measurements and, as such, were used in the validation of transient performance.

3.1 RANGE OF TEST PARAMETERS

The ranges of test parameters over which the critical power tests were conducted are shown in Table 3-3, and separately for the **[ ]**^{a,c} and bottom-peaked tests in Figure 3-4. Histograms displaying the data frequencies in terms of inlet mass flux, outlet pressure, inlet sub-cooling, and lateral power distribution (as reflected by the R-factor) are shown in Figure 3-1 through Figure 3-4.

[

]^{a,c}

3.2 JUSTIFICATION FOR RANGE OF TEST PARAMETERS

The critical power performance of a test bundle is a function of mass flux, pressure, inlet sub-cooling, axial power distribution, and lateral power distribution. The ranges of the test parameters for which the critical power tests were conducted were presented in Section 3.1. Sufficient data coverage is justified in the following subsections.

3.2.1 Mass Flux

Critical power is a strong function of mass flux. Therefore, data were obtained at numerous points **[ ]**^{a,c} over the range of mass flux considered to establish the correlation at various values of pressure, inlet sub-cooling, and bundle lateral powers.

The mass flux was varied from **[** **]**^{a,c}, based on the flow area in the lower section of the test bundle. The typical range of mass flux representing normal operation and AOOs is **[** **]**^{a,c}. The mass flux points obtained cover this expected operating range for **[** **]**^{a,c} test campaigns.

3.2.2 Pressure

[

]^{a,c} This provided sufficient data to determine the system pressure dependence of critical power over the expected range of application of the correlation. Most of the data were obtained at approximately 70 bar (1015 psia) which corresponds to the nominal operating pressure of BWRs.

3.2.3 Inlet sub-cooling

It is well known (see e.g. [2], [3] and [4]) that critical power is a reasonably linear function of the inlet sub-cooling at constant mass flux and system pressure. **[**

]^{a,c} The upper range of inlet sub-cooling covers conditions relevant for the AOO of Loss of Feed-Water Heating.

3.2.4 Axial Power Distribution

The axial power distributions tested should cover relevant conditions experienced by fuel assemblies that can potentially be dryout limiting during normal operation as well as anticipated transients. Below, such relevant axial power distributions are discussed and compared to corresponding selected test conditions in the FRIGG loop.

At the beginning of cycle, during normal operation in a BWR, the axial power shape is skewed towards the bottom of the core as result of voiding. The core designer attempts to improve uranium utilization by making this bottom peak more pronounced and maintaining it as long as possible into the cycle. This increases the average void and allows more Pu-239 to be generated in the top of the core. Towards the end of cycle, when the power gradually shifts to the top of the core due to U-235 depletion at the bottom, the Pu-239 generated is utilized to increase reactivity and thereby prolong the cycle length. Disregarding the local influence of control rods, the level of peaking is typically more extreme in the bottom than in the top of the core. However, partially inserted control rods can locally enhance the top-peaked shape. During the transition from bottom to top-peaked, the power shape may resemble a chopped cosine, but is usually somewhat flatter.

TRITON11 steady-state and transient critical power tests were performed **[** **]**^{a,c} shown in Figure 2-5 and Figure 2-6. The heater rods used in FRIGG have fixed axial power shapes resulting from the manufacturing process. **[** **]**^{a,c}

[

]^{a,c}

[

]^{a,c}

3.2.5 Lateral Power Distribution

When selecting the test matrix, particular emphasis was put on capturing the dependence of critical power on the local (rod-wise lateral) power distribution. The lateral power distributions tested should cover relevant conditions experienced by fuel assemblies that have a reasonable possibility of being dryout limiting during normal operation as well as anticipated transients. Below, such relevant lateral power distributions are discussed and compared to the corresponding selected test conditions in the FRIGG loop.

The lateral heat flux distribution is not significantly altered during fast transients, i.e., in the present context it suffices to consider operation at steady-state and during quasi-stationary conditions. Under such conditions, the main sources of variation in lateral power distribution are: 1) differences in nuclear design, i.e., distributions of U-235 enrichment and Gd concentration across the fuel rod lattice, including effects of isotopic depletion, 2) differences in inter-assembly water gaps between plants, and 3) inserted control rods. In general, the emphasis in the selection of test conditions should be on assemblies that have the possibility of being dryout limiting for the core.

[

]^{a,c}

[1] [ ]^{a,c}

[

]^{a,c}

On the other hand, during the initial phase of Gd depletion, the power is suppressed at and around the Gd rod locations which means that the fuel is usually not dryout limiting. At beginning of life, the power in the Gd rods is approximately 20% of the average rod power. In compensation, the power in other rods is significantly higher than the bundle average, these being typically the peripheral rods facing the fuel channel. The local influence of Gd rods has been studied previously in FRIGG testing of **SVEA-96 Optima3** fuel by selecting lateral power distributions with rod power reduced to approximately 20% at different locations in the bundle. It was shown that the D5 R-factor concept, and thereby the similar D6 concept, is able to correctly model such conditions.

The presence of a zircalloy dummy rod, which may be inserted in place of a failed rod in a repaired fuel bundle, was simulated by cold rods (with zero power) at selected positions.

Bundles adjacent to deeply inserted control rods are usually not dryout limiting. However, realistic power tilts resulting from inserted control rods were included and repeated for all combinations of mass flow, pressure and inlet sub-cooling during the **[ ]^{a,c}**

One advantage of the FRIGG test loop is that the test bundle lateral power distribution can be easily varied. Systematic series of tests were conducted to investigate the critical power performance at various local peaking factors and various peak power rod locations. **TRITON11** critical power measurements were performed with approximately **[ ]^{a,c}** different lateral power distributions with peaking factors [2] between **[ ]^{a,c}** for the full-length/2/3-length/1/3-length rods, respectively. The lateral power distribution obtained differs slightly from the nominal lateral power distribution attempted, since it is the best match that can be obtained with a given rectifier connection. The lateral power distribution actually measured for each data point was used in the correlation development and validation.

In order to determine the dryout sensitivity constants, or "rod constants", in the R-factor model, i.e., the coefficients e_i in Equation 4.5-1, the power was peaked in individual rods starting from an attempted optimized power distribution, in order to push a particular rod into dryout. This process was repeated for all rod locations **[ ]^{a,c}** This is reflected by the number of steady-state dryout occurrences per rod location as shown in Figure 3-5.

As can be seen, essentially all diagonally symmetric rod pairs were taken to dryout when **[ ]^{a,c}**, including some 2/3 and 1/3 PLRs. This enables establishing a complete R-factor model for **TRITON11** fuel. Rods that did not reach dryout were tested at challenging conditions, not far from dryout. As explained in Section 4.6 and validated in Section 5, the D6 R-factor model assumes symmetry for all (most) rods in the outer (second) row and diagonal symmetry for the remaining interior rods of the **TRITON11** fuel rod lattice.

[2] The rod peaking factor is defined as the total (axially integrated) rod power normalized to an average of 1.0 for all **[ ]^{a,c}** rods.

[

]a,c

3.2.6 Combinations of Parameters

To confirm that the parameter ranges considered in the critical power tests cover the combinations of conditions expected during typical reactor applications, the parameter ranges expected during reactor operation are superimposed on the ranges of test points for combinations of parameters to which critical power is considered to be sensitive. As discussed in Section 4, the D6 critical quality is a function of mass flux, pressure, inlet sub-cooling, transformation of axial power profile (I_2), and R-factor. **[**

]a,c

3.2.7 Summary

The discussion of the range of individual parameters in Sections 3.2.1 through 3.2.5 can be summarized as follows. The ranges of parameters shown in Figure 3-1 through Figure 3-4 were selected to cover values of parameters impacting critical power expected during normal BWR operation as well as AOOs and relevant accident scenarios. In selecting the test matrices, greatest emphasis is placed on those regions in which the reactor will usually operate. **[**

]a,c

[

]a,c

The range of lateral power distributions was selected to cover expected conditions during reactor operation and to allow an accurate determination of the dryout sensitivity of each rod in the entire bundle. This was achieved by measurements with approximately [ ]a,c different lateral power distributions.

The data coverage was evaluated in 2-dimensional sub-regions of the computational space of test parameters [ ]a,c and was found to adequately bound the regions of application of the D6 CPR correlation.

3.3 MEASUREMENT DATA VALIDATION CRITERIA AND PROCEDURES

Validation of the measurement data is supported by instrumentation performance reliability checks. All data collection instrumentation is periodically calibrated to assure the accuracy of the data. The data validation process is further reinforced by assuring that all instrumentation is checked for proper operation prior to and at regular instances during each test campaign.

At the beginning of each test campaign a heat balance measurement involving power, mass flow and temperature is performed to confirm that the measurements are accurate and that the assumed power losses in the test section are valid. The verification is performed with the loop top-filled and a pressure being approximately [ ]a,c higher than the saturation pressure for the actual outlet temperature to assure single-phase conditions. Once the FRIGG loop is at stable conditions, measurements with a sampling frequency of [ ]a,c are performed for at least [ ]a,c. The average values of the registered variables are utilized to evaluate the thermal power and electrical power.

The electrical current was measured on both rod level and rectifier level. The current transmitters for all rods were compared with independent measurements by calibrated shunts [ ]a,c times during each test campaign, to verify that they had not drifted (e.g., due to influence from the magnetic field), potentially resulting in biased values. The current was also measured with current frames on rectifier level for rectifier 8, 9, 10 and 11. The rectifier currents were compared to the sum of the rods connected to each rectifier at several occasions during the test campaigns.

The voltage was measured at rectifier level. The power is calculated for all rods from the measured voltage and the current that is measured on rod level and then added up to get the total power of the bundle. The sum of the power generated by each heater rod is compared with the sum of the power outputs from each power supply unit for every data point. These two bundle power measurements must agree within [ ]a,c for the data point to be accepted. The reported bundle power is the one coming from adding all individual rod powers. As mentioned above, the bundle power is corrected for power losses which are verified with heat balance calculations by comparing it to the measured thermal power based on enthalpy rise (from inlet to outlet) and the mass flow rate.

[

]a,c

[

]^{a,c}

Critical power reference test points were repeated to assure that the measurements were stable and reproducible. The reference points for the **TRITON11** test series are defined by the following approximate conditions:

[ ]a,c

[

]^{a,c}

The reproducibility of the critical power was found to be very good for the **TRITON11** test series. Examples of the reproducibility are shown in Table 3-5. The relative standard deviation in measured critical power for each group of data points representing nearly identical conditions is around **[ ]**^{a,c}. When considering the additional variation included due to small differences in the test variables, and the randomness of the dryout transition phenomenon, this is consistent with the estimated accuracy in the measured critical power of **[ ]**^{a,c} (cf. Section 2.5).

Conversion of the data to engineering units by the computer allowed preliminary test validation to be done upon completion of a test run and before the data analysis took place. This preliminary validation provided immediate feedback on facility operation and data collecting equipment performance.

After the instrumentation had been functionally checked, and the test parameters and performance had been compared with the test matrix, the final data validation was performed offline during the data reduction and analysis stage.

3.4 SHIFT IN AXIAL POSITION OF SPACERS

[

]^{a,c}

[

]a,c

3.5 DATA TRENDS

The trends in the experimental data were investigated to confirm that the **TRITON11** critical power database is physically reasonable and consistent with similar measurements obtained for previous fuel assembly designs.

The critical power decreases with a more top-peaked axial power shape. This tendency agrees with measurements obtained for previous fuel assembly designs such as SVEA-96 Optima2 [3] and **SVEA-96 Optima3** [2].

The increasing trend in critical power with increasing inlet sub-cooling, corresponding to reducing inlet temperature, is consistent with results for previous fuel assembly designs. The same well-known linear variation of critical power as a function of inlet sub-cooling, reported in [2] and [3], is also observed for the **TRITON11** design.

The influence of system pressure on critical power at various mass flow rates is similar to previous fuel assembly designs. Critical power is a slowly varying function of pressure with a flat maximum around **[ ]^{a,c}**.

The observations from Figure 3-12 that the axial location of dryout moves towards the outlet at lower mass flows and towards the power peak (location of maximum heat flux) at higher mass flows are well-known and physically motivated. **[**

]^{a,c}

Table 3-1. Number of Data Points per TRITON11 Test Campaign

[ ] a,c

Table 3-2. Number of Data Points per Type of Rectifier Connection

[ ] a,c

Table 3-3. Range of Test Variables Measured and used for D6 Correlation Development

[ ] a,c

Table 3-4. Range of Test Variables and R-factor (Limiting Full-Length Rod)

a,b,c

Table 3-5. Examples of Test Reproducibility

a,c

[ ]a,c

Figure 3-1. Histogram of Data Frequency vs Inlet Mass Flux for [ ]a,c

[ ]a,c

Figure 3-2. Histogram of Data Frequency vs Outlet Pressure for [ ]a,c

[ ]a,c

Figure 3-3. Histogram of Data Frequency vs Inlet Sub-Cooling for [ ]a,c

[ ]a,c

Figure 3-4. Histogram of Data Frequency vs R-factor for [ ]a,c

a,c

Figure 3-5. Number of Steady-State Dryout Occurrences per Rod Location for the [ ]^a,c, respectively

a,c

Figure 3-6. Range of Test Variables, Outlet Pressure vs Inlet Mass Flux, for [ ]^a,c Compared with Typical Application Range

a,c

Figure 3-7. Range of Test Variables, Outlet Pressure vs Inlet Sub-cooling, for [ ]a,c Compared with Typical Application Range

a,c

Figure 3-8. Range of Test Variables, Inlet Sub-cooling vs Inlet Mass Flux, for [ ]a,c Compared with Typical Application Range

[ ]a,c

Figure 3-9. Range of Test Variables, R-factor vs Inlet Mass Flux, for [ ]a,c Compared with Typical Application Range

[ ]a,c

Figure 3-10. Range of Test Variables, Inlet sub-cooling vs R-factor, for [ ]a,c Compared with Typical Application Range.

a,c

Figure 3-11. Range of Test Variables, Pressure vs R-factor, for [ ]^{a,c} Compared with Typical Application Range.

a,c

Figure 3-12. Axial Position of Dryout (measured from onset of heating) vs Inlet Mass Flux for [ ]^{a,c}.

[ ]a,c

Figure 3-13. Axial Position of Dryout (measured from onset of heating) vs Outlet Pressure for [ ]a,c

[ ]a,c

Figure 3-14. Axial Position of Dryout (measured from onset of heating) vs Inlet Sub-cooling for [ ]a,c

a,c

Figure 3-15. Histograms Showing Frequency of Dryout Indications at the Various Axial Positions of Thermocouples (measured from onset of heating) throughout the [ ]a,c Tests

4 D6 CPR CORRELATION MODEL

The D6 CPR correlation for **TRITON11** fuel is a full-bundle correlation in the sense that it is based on full-bundle dryout data and evaluates either the full-bundle minimum CPR or CPR for any of the 109 individual fuel rods. The mathematical expression of the D6 correlation and its application for calculating CPR under steady-state and transient conditions are described in this section. A comprehensive description of the very similar D5 CPR correlation and its use in a wide range of applications is available as a peer-reviewed conference paper [7].

The D6 steady-state CPR correlation describes a best-fit relation, considering the critical power test data, between the critical quality and the parameters of mass flux (with respect to inlet area), outlet pressure, I_2 integral, and R-factor. The I_2 parameter has an implicit dependence on inlet sub-cooling and mass flow through the integration length which equals the boiling length. The influence of local power peaking on CPR is incorporated via an exponential dependence of the critical quality on the R-factor. The detailed critical quality expression is given in Section 4.3 and the R-factor model is described in Section 4.5.

A least squares method was used to optimize the correlation and R-factor coefficients by systematically minimizing the difference between the predicted and measured dryout power for the steady-state dryout data points obtained in FRIGG. The basis for this optimization was the variation of inlet mass flux, outlet pressure, inlet sub-cooling, axial power profile, and lateral rod power distribution investigated with the FRIGG database.

For transient applications, the same correlation function is used but with a change to a Lagrangian coordinate that follows each film fluid particle, as described in [2].

All parameters discussed below are in SI units unless otherwise stated.

4.1 SELECTED CORRELATION FORM

Theoretical considerations of the dryout phenomenon were used to derive the relevant parameters in the determination of critical power under various conditions, with emphasis on the influence of axial power shape captured through the I_2 integral. Also, as described in Section 5.1 of [2], physical considerations and empirical data trends from FRIGG testing of **SVEA-96 Optima3** were used to derive the D5 correlation form.

Here it suffices to mention that the D6 CPR correlation model for **TRITON11** fuel inherits the same basic correlation form as the D5 CPR correlation used for **SVEA-96 Optima3** fuel. The expressions for critical quality as function of mass flux, pressure, inlet sub-cooling, axial power distribution, and R-factor are identical. **[**

]^{a,c} For robustness there is a desire to reduce the number of fitting coefficients to the bare minimum needed.

The differences between the D5 and D6 CPR correlations, apart from assigning new values to the coefficients by fitting against the corresponding FRIGG data, are solely in the R-factor formulation. In

---

1 **[** **]**^{a,c}

addition to the obvious expansion from 5×5 to 11×11 rod lattice geometry, the D6 R-factor model includes a **[**

]^{a,c}

4.2 EXTRAPOLATION IN MASS FLUX

Westinghouse has found that under certain circumstances it may be necessary to evaluate critical power outside of the mass flux range which can be covered by experiments in FRIGG. For example, in some plant applications, critical power evaluation may be needed at very low core flows for which assemblies on the core periphery could have the potential for experiencing mass flux values less than **[**

]^{a,c}. Application of the correlation to very low flows is also necessary during certain dynamic events. Therefore, it may be necessary to conservatively estimate **TRITON11** critical power values for mass fluxes outside of the range used in the development of the correlation. The critical power estimates outside of the correlation range from **[** **]**^{a,c} must be established conservatively since measurement data for **TRITON11** fuel are not available for validation outside of this range.

Critical power tests demonstrate that critical quality increases with decreasing mass flux. This is demonstrated in the response to RAI-SNPB-25 of [2]. Therefore, conservative critical powers are predicted at all mass fluxes between **[**

]^{a,c}

For all fuel designs tested, including the **TRITON11** design, critical power has been found to be a **[**

]^{a,c}

The manner in which the D6 CPR correlation will be applied to licensing-based analyses is summarized as follows:

[**]** **a,c**

4.3 D6 STEADY-STATE CPR CORRELATION

The steady-state CPR for a **TRITON11** bundle is defined in the usual manner as:

[ ] a,c (4.3-1)

where:

Q_{actual} = Actual bundle power

[ ] a,c (4.3-2)

where

ε = Iteration convergence limit (typically 2×10^{-4}).

[ ] a,c

Having determined the bundle critical power, Q_c, to satisfy Equation 4.3-2, an axial distribution of CPR in the **TRITON11** bundle can be considered as:

[ ] a,c (4.3-3)

Note that $\min_z\{CPR(z)\} = CPR_{min}$ per construction.

The D6 steady-state critical quality is defined as:

[ ]a,c (4.3-4)

where

[ ]a,c
(4.3-5)

(4.3-6)

a,c

and

[ ]

The global D6 CPR correlation coefficients are given as:

[ ]a,c

The remaining coefficients used in the D6 R-factor model are defined in Section 4.5.

[

]a,c

Each of the optimized functional forms defining the D6 critical quality are plotted in Figure 4-1 through Figure 4-4 using typical operating conditions (for the fixed parameters) and over a range wider than the correlation development range defined in Table 5-5. In each case, the bounding critical quality functions (i.e., least and most limiting within the correlation development range) are also plotted. As indicated in Figure 4-1 through Figure 4-4, all functions are continuous and well behaved over the correlation range of validity. The ranges over which the D6 correlation is valid are provided and justified in Section 5.

4.4 D6 TRANSIENT CPR CORRELATION

The transient D6 CPR correlation is a generalization of the steady-state D6 CPR correlation defined in Section 4.3. It is based on the same correlation expression with the same empirical coefficients. Under steady-state conditions, the two correlations are equivalent. The R-factor determined at the transient initial condition is kept constant throughout the transient.

Transient I_2 integral

[

]^{a,c}

Mass flux

The instantaneous outlet mass flux seen by the film fluid particle at the instant when it exits the bundle was selected for the transient D6 CPR correlation. This mass flux is normalized to the inlet flow area for consistency with the steady-state approach.

Pressure

Consistent with the definition of the transient mass flux and the steady-state approach, the corresponding (instantaneous) steam properties at the outlet were selected for the dependence on pressure.

The performance of the D6 CPR correlation has been investigated for various types of transients. The behavior with time is always smooth, indicating stability with respect to small increments as ensured by the simple form of the correlation function (everywhere differentiable). **[**

]^{a,c}

4.5 D6 R-FACTOR

The R-factor accounts for the influence of the local power distribution (relative rod power distribution in the bundle), cross section geometry, and the spacer grid design and configuration. The traditional R-factor concept used, e.g., in the D4.1 correlation for SVEA-96 Optima2 fuel [3] is basically two-dimensional (2D) and assumes that the axial and radial power distributions within the (sub-)assembly are separable (i.e., all fuel rods have the same axial power distribution). To deal with, e.g., partially controlled assemblies, ad hoc weighting schemes were developed to combine the R-factors from different axial cross sections. With the introduction of PLRs this modeling practice became increasingly cumbersome and tedious to handle.

4.5.1 Generalized R-factor Model

A generalized, fully three-dimensional (3D) R-factor model was developed for the D5 CPR correlation used with **SVEA-96 Optima3** fuel [2]. The same basic concept is used for the D6 CPR correlation. The numbering of fuel rods in the **TRITON11** bundle is done according to Figure 2-4, i.e., numbering starts from the control rod (NW) corner. The D6 R-factor for an individual fuel rod, *i*, at axial position, *z*, takes the following form:

a,c

[

]a,c

[

]a,c

[2] In case of a sub-bundle power mismatch, this results in a lower than average inlet mass flux to the hottest sub-assembly. The sub-bundle CPR model is described in Section 3.2.1 of [3].

The calculation of CPR for individual fuel rods is based on the above rod specific R-factors. The calculation of the bundle minimum CPR is based on the maximum of all individual rod R-factors in each axial cross section,

$$R(z) = max_i\{ R_i(z)\} \tag{4.5-4}$$

The coefficients for the D6 R-factor model are given by:

[ ]a,c

The rod constants (e_i) are given in Table 4-1.

A convenient numerical property of the D6 bundle R-factor is that its theoretical lower limit is determined by the average of the rod constants for full-length rods, $<1+e_i>$ = 1.000. The rod constants quantify the influence of cross-section geometry and spacer grid design on the relative rod-to-rod dryout sensitivity, as determined in the dryout tests. These differences in dryout sensitivity are generally small as a result of an optimized spacer design. Lower values of the rod constants correspond to better dryout performance.
[

]a,c. As for **SVEA-96 Optima3**, the rod constants are applied multiplicatively as opposed to additively as in previous R-factor models. This is to ensure that all rods, in particular the PLRs, are treated consistently in terms of extrapolation of their R-factors with rod power.

It should be noted that the linear heat generation rate, $q_i(z)$, represents the true 3D power distribution of the bundle, and not the set of normalized 2D power distributions that were used in older R-factor models (see e.g., [3]).

[

]a,c

[ ]a,c (4.5-5)

4.5.2 Treatment of Part-Length Rods

[

]a,c

4.5.3 Use of Pin Power Reconstruction

For CPR correlations prior to D5, the R-factors used in core design and core supervision were pre-calculated based on idealized (fixed void and reflective single-assembly boundary) conditions evaluated with a 2D lattice code (e.g., PHOENIX4 [5]). This simplified approach is no longer needed with the D5 and D6 CPR correlations. The generalized D6 R-factor model can utilize the complete 3D (relative) pin power distribution in the bundle as calculated with a pin power reconstruction technique, e.g., as available in POLCA7 [5], or another licensed 3D core simulator. The power distribution is no longer required to be separable into axial and radial components. In this way, the CPR calculation accounts for local power perturbations from surrounding core components such as:

- Heterogeneities in assembly reactivity (mainly due to differences in burnup for neighboring bundles).
- Control rods inserted in neighboring cells.
- Neutron leakage at the core periphery.

This allows a more accurate determination of the CPR for individual assemblies as well as the limiting CPR for the core.

The effects of using pin power reconstruction for CPR evaluation are demonstrated in [7].

[

]a,c

4.6 DETERMINATION OF D6 COEFFICIENTS

[

]a,c

A least squares method was used to optimize the correlation and R-factor coefficients by systematically minimizing the sum of square differences between the predicted and measured critical power. The basis for this optimization was the variation of inlet mass flux, outlet pressure, inlet sub-cooling, axial power profile, and lateral rod power distribution studied in the steady-state FRIGG database.

The general fitting procedure was as follows.

[

]a,c

3 [

]a,c

[

]a,c (4.6-1)

Table 4-1. Rod constants (e_i) for D6 R-factor Model (shaded numbers for PLRs)

a,c

a,c

Figure 4-1. D6 Critical Quality Dependence on Inlet Mass Flux (typical and bounding functions) within and outside the Database Limits Indicated by Dashed Lines

a,c

Figure 4-2. D6 Critical Quality Dependence on Outlet Pressure (typical and bounding functions) within and outside the Database Limits Indicated by Dashed Lines

a,c

Figure 4-3. D6 Critical Quality Dependence on $I_{2,m}$ (typical and bounding functions) within and outside the Database Limits Indicated by Dashed Lines

a,c

Figure 4-4. D6 Critical Quality Dependence on R-factor (typical and bounding functions) within and outside the Database Limits Indicated by Dashed Lines

a,c

Figure 4-5. Example of Axial Distributions of Critical (X_c) and Iterated (X_{it}) Steam Qualities for a Bundle with Bottom-Peaked Axial Power Distribution, where the Bundle Minimum CPR occurs at 2/3 Axial Level due to a 2/3-length Rod with High Power

5 D6 STEADY-STATE CPR VALIDATION

Validation of the D6 CPR correlation relative to the steady-state database is performed in this section. The validation against transient critical power measurements is presented in Section 6.

The present D6 steady-state CPR database is composed of **[ ]^{a,c}** test points measured with a **TRITON11** bundle, of which **[ ]^{a,c}** were used for development of the correlation. The number of data points and lateral power distributions for each axial power distribution were summarized in Table 3-1. The five categories (Types 1-5) of data points defined in the beginning of Section 3 and quantified in Table 3-2 are referred to below.

In Section 5.1, the absence of significant trends in the prediction errors and expected critical power dependences are demonstrated. In Section 5.2, the final correlation mean and standard deviation errors to be used in safety analysis are determined by training the correlation on only **[ ]^{a,c}** of the development database and reserving the remaining **[ ]^{a,c}** for validation. In Section 5.3, the domains of development and application of the correlation in terms of ranges in the main correlation variables are established.

Note that due to the nature of the CPR correlation assumptions under steady-state conditions (based on equilibrium state in closed channels), this validation and associated statistics are independent from the computer code in which the correlation has been implemented (neglecting small differences due to considered nodalization and water properties). This is unlike the correlation validation for transient applications (see Section 6.2).

5.1 D6 PERFORMANCE RELATIVE TO FRIGG DATABASE

The D6 CPR prediction error is given by:

$$\text{Prediction Error [\%]} = \left[\frac{\text{predicted critical power}}{\text{measured critical power}} - 1\right] \times 100 \qquad (5.1\text{-}1)$$

Table 5-1 gives the mean prediction error and standard deviation of prediction error considering the entire database of **[ ]^{a,c}** data points used for correlation development. **[**

]^{a,c}

The histogram of prediction error frequency for the development database is shown in Figure 5-1. As indicated, the prediction errors are adequately represented by a normal distribution. The mean prediction error is zero per construction. The standard deviation error is **[ ]^{a,c}**.

The predicted critical powers vs measured critical powers are shown in Figure 5-2. The solid lines in this figure represent deviations of ±5%. Table 5-2 provides the number and percentage of data points outside the ±5% boundaries.

A useful graphical validation technique is to study the trends of the prediction error (Equation 5.1-1) vs the main correlation variables. A perfect prediction is characterized by zero prediction error. A negative (positive) prediction error is conservative (non-conservative) in the sense that critical power is under-predicted (over-predicted) by the correlation model as compared to the measured critical power.

In Figure 5-3 through Figure 5-7, the D6 prediction error is plotted as function of **[**

]^{a,c}. No significant biases or trends are found in the prediction errors.

[

]^{a,c}

Similarly, Figure 5-15 shows the critical power dependence on inlet sub-cooling for several different mass flux values. As can be seen, the D6 CPR correlation predicts **[**

]^{a,c}

In summary, the following conclusions can be drawn from the evaluation of the D6 CPR correlation predictions over the **[** **]**^{a,c} databases:

1. All physical trends in the critical power database discussed in Section 3 are adequately captured with the D6 CPR correlation. Furthermore, the predicted critical power trends **[** **]**^{a,c} are consistent with previous dryout testing of earlier fuel assembly designs.

2. The D6 CPR correlation predictions show no evidence of significant biases or trends relative to the **[** **]**^{a,c}

5.2 CORRELATION MEAN AND STANDARD DEVIATION ERRORS

Data used to determine the correlation predictive uncertainty (i.e., validation data) should not be used to train the correlation, as the correlation will predict training data with more accuracy than it would predict data it has never seen. For this reason, the database used for optimizing the D6 correlation coefficients was divided into two random subsets with **[ ]a,c** data points **[ ]a,c** for training and **[ ]a,c** data points **[ ]a,c** for validation, respectively. This process was repeated **[ ]a,c** times. For each random trial, the main correlation coefficients **([ ]a,c** in Equations 4.3-4 and 4.3-5) were re-optimized using only the training dataset. The R-factor was kept unchanged. The mean and standard deviation prediction errors were calculated separately for the training and validation datasets. The sample average results are given in Table 5-4 and were well converged with **[ ]a,c** trials as can be seen in Figure 5-16.

As expected, the sample average standard deviation from validation **[ ]a,c** is slightly larger than the sample average standard deviation from training **[ ]a,c**, the difference being only **[ ]a,c**. In comparison, the sample average standard deviation from all **[ ]a,c** data points is **[ ]a,c**, i.e., the same (within two digits) as obtained in Section 5.1 from the correlation development. The sample average mean error from validation shows a very small negative bias of **[ ]a,c** which is (conservatively) neglected.

In summary, the following correlation statistical parameters will be conservatively assumed in evaluations of SLMCPR:

D6 CPR Correlation Uncertainty (standard deviation error) = **[ ]a,c** (5.2-1)

D6 CPR Correlation Bias (mean error) = **[ ]a,c** (5.2-2)

5.3 RANGE OF APPLICABILITY

The range over which a CPR correlation is traditionally valid corresponds to the experimental range over which the correlation was developed and yields the claimed statistical performance (i.e. mean value and standard deviation). This development range is provided in Table 5-5. Correlation applicability outside this range can however be justified (1) by conservatively bounding the critical power based on known monotonous asymptotic behavior of the physical phenomena or (2) by comparing the correlation performance to a physical model of the dryout event in the same rod bundle geometry over the targeted application range.

The range of applicability for the mass flux has been discussed in Section 4.2 where the bounding method (1) was used at low flow (by limiting the critical quality) and high flow (by limiting the critical power) beyond the FRIGG experimental database. In Sections 5.3.1 and Section 5.3.2, the applicability ranges for the transformation of axial power profile (I_2) and the R-factor are discussed. The limits of validity of the D6 CPR correlation are given in Table 5-6.

5.3.1 Consideration of Axial Power Distribution (I_2)

[

]a,c

[

]a,c

5.3.2 Consideration of Lateral Power Distribution

The adequacy of the lateral power distributions tested was discussed in Section 3.2.5.

[

]a,c

[

]^{a,c}

5.3.3 Final Ranges of Applicability

The final ranges over which the D6 CPR correlation is valid are shown in Table 5-6. These ranges are based on the **[ ]^{a,c}** steady-state data points used for correlation development. **[ ]^{a,c}** are explicit input variables to the D6 CPR correlation and will be monitored during licensing applications to assure that they stay within the applicable range of the D6 CPR correlation.

[

]^{a,c}

Table 5-1. Mean Prediction Error and Standard Deviation Error for D6 CPR Correlation Considering the Entire Development Database

a,b,c

Table 5-2. Number and Percentage of Data Points Exceeding ±5% Prediction Error for D6 CPR Correlation

a,b,c

Table 5-3. Statistics of D6 CPR Correlation Predictions for Various Data Subsets

[ ]a,b,c

Table 5-4. Average over [ ]a,c Samples of Mean Prediction Error and Standard Deviation Error for Training and Validation Databases

[ ]a,b,c

Table 5-5. Development Range for D6 CPR Correlation

a,b,c

Table 5-6. Validity Range for D6 CPR Correlation

a,b,c

a,b,c

Figure 5-1. Histogram of D6 Prediction Errors for D6 CPR Correlation Considering the Entire Development Database

a,b,c

Figure 5-2. Predicted vs Measured Critical Power for D6 CPR Correlation Applied to [ ]^{a,c} – the Lines Represent ±5% Error

a,b,c

Figure 5-3. D6 Prediction Error as Function of Inlet Mass Flux for [

]a,c

a,b,c

Figure 5-4. D6 Prediction Error as Function of Outlet Pressure for [

]a,c

a,b,c

Figure 5-5. D6 Prediction Error as Function of Inlet Sub-cooling for [ ]^{a,c}

a,b,c

Figure 5-6. D6 Prediction Error as Function of Modified Axial Power Profile Transformation, $I_{2,m}$, for [ ]^{a,c}

a,b,c

Figure 5-7. D6 Prediction Error as Function of R-factor for [ ]a,c. Data Points with a 1/3 or 2/3-PLR being Predicted as Limiting for CPR are Indicated.

a,b,c

Figure 5-8. D6 Prediction Error as Function of Inlet Mass Flux at Off-Nominal Pressures

a,b,c

Figure 5-9. D6 Prediction Error as Function of Inlet Sub-cooling at Off-Nominal Pressures

a,b,c

Figure 5-10. D6 Prediction Error as Function of Inlet Mass Flux at Off-Nominal Inlet Sub-cooling

a,b,c

Figure 5-11. D6 Prediction Error as Function of Inlet Mass Flux in Different R-factor Ranges

a,b,c

Figure 5-12. D6 Prediction Error as Function of Outlet Pressure in Different R-factor Ranges

[ ]a,b,c

Figure 5-13. D6 Prediction Error as Function of Inlet Sub-cooling in Different R-factor Ranges

[ ]a,b,c

Figure 5-14. D6 Critical Power Dependence on Mass Flux Predicted for the FRIGG [ ]a,c

a,b,c

Figure 5-15. D6 Critical Power Dependence on Inlet Sub-cooling Predicted for the FRIGG [ ]a,c

a,b,c

Figure 5-16. Running Average over [ ]a,c Samples of Mean and Standard Deviation Errors from Training and Validation Databases

6 D6 TRANSIENT CPR VALIDATION

6.1 INTRODUCTION

One specified acceptable fuel design limit (SAFDL) is that no more than 0.1% of the fuel rods in the core are allowed to experience boiling transition during an AOO and during normal operation. This requirement is typically satisfied by evaluating the change in CPR (ΔCPR) during licensing basis AOOs and establishing a CPR operating limit such that the SLMCPR will not be violated during limiting transient events.

Transient CPR predictions involve evaluation of the flow, enthalpy, and pressure in the fuel assembly at each axial node as a function of time during the transient. A transient system analysis code is used to calculate the transient fluid parameters. These parameters are then used with an assembly-specific CPR correlation to evaluate transient CPR. One transient system analysis code used by Westinghouse for CPR predictions is the BISON-SLAVE channel model of the BISON transient analysis code documented in [1].

The methodology for demonstrating that the application of the D6 CPR correlation in transient calculations will provide adequate predictions of the onset of dryout is described in this section. Specifically, the process for validating the D6 dryout prediction performances in any transient code is first presented. Then, the transient dryout experiments performed in the FRIGG test loop with the **TRITON11** fuel geometry are described. Finally, the validation of the D6 CPR correlation using the BISON-SLAVE transient code is presented.

6.2 TRANSIENT VALIDATION METHODOLOGY

The two objectives of the transient system analysis code validation, with respect to dryout prediction, are to:

1. Confirm proper implementation of the transient CPR correlation in the transient code.

2. Confirm the capability of the transient code along with the transient CPR correlation to predict dryout during transients with adequate accuracy.

The transient dryout performance of a CPR correlation is validated for each fuel bundle design and code application by confirmation of accurate predictions relative to experimental steady-state and transient dryout data. The performance dependency on the selected code is due to potential differences in transient response driven by differences in closure models (e.g. phase velocity slip) and associated relaxation times. The validation is performed by simulating all available transient dryout tests and verifying that:

a,c

[

]^{a,c}

6.3 TRANSIENT DRYOUT EXPERIMENTS

The considered transient dryout data were taken in controlled transient experiments performed in the FRIGG test loop with the **TRITON11** fuel geometry. The measurements were performed for **[**]^{a,c} and included different initial parameter variations as well as various transient event simulations.

6.3.1 FRIGG Loop

Power increase transients, flow reduction transients and combinations of power and flow transients are simulated in the FRIGG loop transient tests. The selected transient cases are **[**

]^{a,c}

A power supply controller, capable of producing power pulses providing heat flux variations which simulate BWR fast pressurization events, was used for the transient test simulations. Rapid test loop flow reductions, which are needed to simulate the very fast flow reductions in BWRs with internal pumps, were accomplished by modulating the pump speed. Relative changes in power and flow were generated according to the profiles shown in Figure 6-1 and Figure 6-2.

Dynamic heater rod TC responses were recorded as function of time during the transient tests. In addition, transient test system response data were recorded in order to provide time-dependent boundary conditions for the transient system code simulations. The test section **[**]^{a,c}

6.3.2 Test Section

The same **[**]^{a,c} test sections as used for the steady-state testing described in Section 2 were used for the transient tests.

6.3.3 Transient Test Description

The **TRITON11** transient tests can be categorized as power increase, flow reduction or combination transients for various transient power and flow histories, and test section flow rates. All tests were performed for an **[**]^{a,c}. Each test was performed with the **[**]^{a,c} shown in Table 2-2 and Table 2-3. A total of **[**]^{a,c} transient tests were performed. Of these, 45 tests are classified as power increase transients, **[**]^{a,c} tests are characterized as flow reduction transients and **[**]^{a,c} tests are combination tests.

[

]^a,c The power and inlet flow transient profiles shown in Figure 6-1 and Figure 6-2 are normalized to initial values. The actual measured values of [

]^a,c

Table 6-1 and Table 6-2 provide a summary of the test conditions for each transient. The results of each test and the corresponding predictions of BISON/SLAVE are summarized in Table 6-3 and Table 6-4.
[

]^a,c

Table 6-1 and Table 6-2 describe tests with [

]^a,c

6.3.4 Experimental Dryout Determination

During a transient, the rod temperature typically varies first with heat flux (pre-dryout phase), then increases rapidly (dryout and post-dryout phase) before decreasing suddenly due to power reduction and associated rod rewetting (quenching phase). These characteristics can be utilized to detect (1) if transient dryout has occurred and (2) the onset and duration of dryout.

[

]^a,c

6.3.5 Transient Data

Example test boundary conditions for a power increase test (Test number 1364-1), a flow reduction test (Test number 1476-1) and a combination test (Test number 1332-1) are shown in Figure 6-3, Figure 6-5 and Figure 6-7, respectively. These figures show the test section power and coolant inlet flow as functions of time (which are used as boundary conditions in the transient code simulations). The corresponding measured limiting rod temperature responses are shown in Figure 6-4, Figure 6-6 and Figure 6-8, respectively. [ ]^a,c

[

]a,c

For the power increase without a flow decrease transient shown in Figure 6-3 and Figure 6-4, the flow variations that occur are due to the heat flux changes (and associated pressure drop change) created by the power transient, rather than to changes induced by recirculation flow.

Test number 1476-1 is an example of a **[**

]a,c

It should be noted that the entire signal recording time range is not shown in Figure 6-3 through Figure 6-8. Only 8 seconds of the transients are shown, of which about 2 seconds is initial steady-state operation.

The temperature traces shown in Figure 6-4, Figure 6-6 and Figure 6-8 are provided to illustrate the type of temperature responses for typical test power and flow histories used in the **TRITON11** tests. Such plots provide physical insight into the transient response to the test boundary conditions and assure that any anomalies are detected.

6.4 IMPLEMENTATION VALIDATION FOR BISON CODE

The BISON-SLAVE channel model in the time domain reactor dynamics code BISON [1] will be used in conjunction with the D6 CPR correlation to predict transient CPR behavior for licensing analysis applications. The BISON-SLAVE simulations presented in this section illustrate the application of the methodology described in Section 6.2 for confirming that the D6 transient CPR correlation is acceptable for transient applications.

An overview of the BISON code and test section model is given below. The transient test simulation results are compared with the measurements in Section 6.4.3.

6.4.1 BISON Code

BISON is a time domain BWR dynamics code used for analyzing operational and safety related transients. The code simulates the hydraulics of the entire primary core coolant loop including the recirculation pumps. A two-group diffusion theory model describes the axial distributions of neutron flux and power in the reactor core. Heat conduction in the fuel is solved in the radial direction at each axial segment. The influence from external systems such as the turbine, control systems, scram signals, and relief valves can also be simulated in BISON.

The BISON-SLAVE module of the code is used for the simulation of a single bundle in the core by utilizing boundary conditions from a BISON system calculation for the entire reactor. It can also be used in a stand-alone mode to study heated bundles in test loop experiments. External boundary conditions in the form of inlet mass flow and temperature, inlet pressure, and assembly power are supplied as input to the code. This option was used in the present evaluation to calculate the transient CPR for the experiments performed.

The D6 transient CPR correlation is incorporated in the BISON-SLAVE code. [

]^{a,c}

6.4.2 BISON Model

The [ ]^{a,c} are modeled in the BISON simulations of the tests. The heated part of the test section is simulated with the BISON-SLAVE channel model. The heater rod is modeled with the same radial nodal divisions typically used in plant calculations. The radial representation and material compositions of the heater rod are shown in Figure 6-9.

The experimental conditions described in the previous sections were used as input to the BISON-SLAVE model. The test assembly [

]^{a,c}

The CPR during the transient is calculated using the transient D6 CPR correlation (see Section 4.4) implemented in the BISON code.

6.4.3 BISON Test Simulation Results

All [ ]^{a,c} transient tests were simulated with the BISON-SLAVE code. The experimental determination of whether or not dryout occurred and the predicted minimum CPR for each test are listed in Table 6-3 and Table 6-4. Figure 6-10 and Figure 6-11 show the minimum CPR predicted by the BISON-SLAVE simulations compared to the detected dryout status from the measurements for all tests. The frequency distributions of predicted minimum CPR are presented in Figure 6-12 and Figure 6-13. Dryout is determined from the temperature measurements using the methodology described in Section 6.3.4 and predicted by the BISON-SLAVE simulation with a CPR criterion of less than or equal to 1.0. A non-conservative BISON-SLAVE prediction occurs when the dryout is determined by the test, but not by the simulation (i.e., minimum CPR > 1.0).

[

]^{a,c}

6.5 SUMMARY

The Westinghouse methodology for application of a CPR correlation for transient simulations was illustrated in this section using the D6 transient CPR correlation and the BISON-SLAVE channel model. Comparisons of BISON-SLAVE code predictions with **TRITON11** full-bundle test results demonstrated that the D6 transient CPR correlation is capable of providing accurate determination of the onset of dryout during transients. It is concluded that the D6 transient CPR correlation used in the BISON-SLAVE channel model provides accurate predictions of the transient dryout test data. It can be concluded that the D6/BISON-SLAVE combination will not underestimate the CPR response of the operational transients to which it will be applied and will support conservative CPR operating limits.

Table 6-1. [ ]a,c

a,b,c

Table 6-1. [ ]a,c (cont.)

a,b,c

Table 6-2. [ ]a,c

a,b,c

Table 6-2. [ ]^{a,c} (cont.)

a,b,c

Table 6-3. [ ]a,c Test Results and BISON/SLAVE Predictions

a,b,c

[ ]

Table 6-3. [ ]a,c Test Results and BISON/SLAVE Predictions (cont.)

a,b,c

Table 6-4. [ ]a,c Test Results and BISON/SLAVE Predictions

a,b,c

Table 6-4. [ ]a,c Test Results and BISON/SLAVE Predictions (cont.)

a,b,c

a,b,c

Figure 6-1. Power-Time Profiles

a,b,c

Figure 6-2. Flow-Time Profiles

a,b,c

Figure 6-3. Power Increase Transient – Experiment Number 1364-1 – Power and Mass Flow

a,b,c

Figure 6-4. Power Increase Transient – Experiment Number 1364-1 – Measured Temperature

a,b,c

Figure 6-5. Flow Reduction Transient – Experiment Number 1476-1 – Power and Mass Flow

a,b,c

Figure 6-6. Flow Reduction Transient – Experiment Number 1476-1 – Measured Temperature

a,b,c

Figure 6-7. Combination Transient – Experiment Number 1332-1 – Power and Mass Flow

a,b,c

Figure 6-8. Combination Transient – Experiment Number 1332-1 – Measured Temperature

a,b,c

Figure 6-9. BISON-SLAVE Model for Test Heater Rod

a,b,c

Figure 6-10. Transient Validation for [ ]^{a,c} Power Shape

a,b,c

Figure 6-11. Transient Validation for [ ]^{a,c} Power Shape

a,b,c

Figure 6-12. Transient Validation for [ ][a,c] – Histogram of Predicted CPR Distribution for the [ ][a,c] Power Shape

a,b,c

Figure 6-13. Transient Validation for [ ][a,c] – Histogram of Predicted CPR Distribution for the [ ][a,c] Power Shape

7 CONCLUSIONS

The critical power measurements described in the present report provide an accurate simulation of the dryout performance of the **TRITON11** fuel assembly. A total of **[ ]a,c** steady-state data points covering the entire range of expected reactor operating conditions were obtained. In addition, a total of **[ ]a,c** transient measurements representative of BWR transients were obtained. The D6 CPR correlation was developed based on **[ ]a,c** of the steady-state data points.

The aim of the correlation development was to provide best-estimate prediction of steady-state critical power and accurate prediction of transient critical power for a **TRITON11** fuel assembly. The steady-state mean prediction error and standard deviation over the entire range of validity are **[ ]a,c**, respectively. The correlation uncertainty is preferably incorporated in the evaluation of SLMCPR and OLMCPR by a normal distribution with mean value of **[ ]a,c** and standard deviation of **[ ]a,c**

Based on the critical power data for **TRITON11** and the evaluations of the data presented in this report, the following conclusions can be drawn:

1. Sufficient data have been obtained and sufficient analysis has been performed to justify the use of the D6 CPR correlation for design and licensing applications over the following input variable ranges:

[ ]a,b,c

2. The D6 CPR correlation provides best-estimate prediction of the steady-state CPR.

3. The D6 CPR correlation provides accurate prediction of CPR during transient conditions.

The correlation has been demonstrated to be capable of providing accurate estimate of the onset of dryout during fast transients. This capability must be evaluated for each transient system code application. It was demonstrated that the correlation, in conjunction with the BISON-SLAVE code, is acceptable for the calculation of changes in CPR during transient events for design and licensing applications.

8 REFERENCES

[1] Westinghouse CENPD-292-P-A (Proprietary), CENPD-292-NP-A (Non-Proprietary), "BISON – One Dimensional Dynamic Analysis Code for Boiling Water Reactors: Supplement 1 to Code Description and Qualification," July 1996.

[2] Westinghouse Report WCAP-17794-P-A (Proprietary), WCAP-17794-NP-A (Non-Proprietary), "10x10 SVEA Fuel Critical Power Experiments and New CPR Correlation: D5 for **SVEA-96 Optima3**," September 2020.

[3] Westinghouse Report WCAP-16081-P-A (Proprietary), WCAP-16081-NP-A (Non-Proprietary), "10x10 SVEA Fuel Critical Power Experiments and CPR Correlation: SVEA-96 Optima2," March 2005.

[4] Westinghouse Report CENPD-389-P-A (Proprietary), CENPD-389-NP-A (Non-Proprietary), "10x10 SVEA Fuel Critical Power Experiments and CPR Correlations: SVEA-96+," September 1999.

[5] Westinghouse Report CENPD-390-P-A Rev. 0 (Proprietary), CENPD-390-A Rev. 0 (Non-Proprietary), "The Advanced PHOENIX and POLCA Codes for Nuclear Design of Boiling Water Reactors," December 2000.

[6] F. Waldemarsson, J.-M. Le Corre and U. C. Bergmann, "**TRITON11** BWR fuel thermal-hydraulics testing overview, challenges and models," *19th International Topical Meeting on Nuclear Reactor Thermal Hydraulics* (NURETH-19), Brussels, Belgium, March 6 – 11, 2022.

[7] U.C. Bergmann, C. Adamsson, and G. Norbäck, "Advanced dryout correlation and CPR methodology for Westinghouse **SVEA-96 Optima3** fuel," in proceedings of Advances in Nuclear Fuel Management IV (ANFM 2009), Hilton Head Island, SC, USA, April 12-15, 2009.

[8] NUREG/KM-0013, *Credibility Assessment Framework for Critical Boiling Transition Models: A generic safety case to determine the credibility of critical heat flux and critical power models*, Draft for Comment, March 2019.